

Spatially varied miaroles in the albite porphyry of Cuchillo Mountain, southwestern New Mexico

KENT McMILLAN

Geosciences Group, Basalt Waste Isolation Project, Rockwell Hanford Operations, Richland, Washington 99352

ABSTRACT

Miarolitic segregations in the albite porphyry of Cuchillo Mountain become increasingly complex mineral aggregates as they are traced inward from the intrusive margins. Segregations in the outer portions of the intrusion are characterized by quartz-alkali feldspar aggregates \pm epidote, chlorite, quartz, and carbonate; the interior portion, by epidote, quartz, and carbonate \pm alkali feldspar. The composition of the interior miaroles is compatible with a pervasive albite-epidote-chlorite replacement assemblage, from which the albite porphyry is derived. The earliest and latest miaroles bracket the replacement assemblage, indicating that the alteration was a late magmatic effect.

The miarolitic segregations can be correlated with inward consolidation and reflect the proportionately more complete segregation of hydrous melt and vapor phase in the interior. Interior miaroles exhibit textures and compositional trends in epidote similar to those observed in tourmaline from pegmatite gem pockets. The general course of development of the miarolitic segregations parallels the inferred development of granitic pegmatite systems: crystallization from hydrous melt, then from hydrous melt and vapor, and finally essentially from vapor.

INTRODUCTION

Postemplacement miarolitic segregations vary texturally and mineralogically with respect to position in the albite porphyry intrusion underlying Cuchillo Mountain (Fig. 1). Near the intrusive margins, the segregations are relatively small, simple intergroundmass aggregates of quartz and alkali feldspar. Toward the interior, the segregations are larger and more complex. In the core region, several types of segregations are represented including miaroles up to 3.0 cm in diameter with well-developed crystal-filled cavities. This sequence of inward-increasing size and complexity is correlated with consolidation inward from the margins and hence records a temporal as well as a spatial sequence analogous with pegmatite development, i.e., early crystallization from hydrous melt, followed by crystallization from hydrous melt and vapor, and, finally, crystallization from a vapor-dominated system. Some features of the interior miaroles are similar to features found in pegmatite gem pockets.

The purpose of this paper is to describe the paragenesis of the miarolitic segregations and discuss their origins in terms of the pegmatite model described by Jahns and Burnham (1969) and Jahns (1982), emphasizing the role of cooling rate in controlling the segregation of hydrous melt and vapor.

PETROLOGIC SETTING

The albite porphyry intrusion is a subvolcanic, semi-concordant mass, emplaced within a thick carbonate sequence [see Jahns et al. (1978) for description of the geo-

logic setting] and pervasively altered from andesine monzonite porphyry to albite porphyry (McMillan and Jahns, 1978). The origin of the alteration is endogenic, as it is bracketed in time by the earliest and latest miarolitic segregations. Moreover, the alteration is restricted in its distribution to the intrusive mass; it is not present in the host rock section. The completeness of the alteration increases from the margins toward the interior and involves the formation of albitic feldspar, epidote, and chlorite after the primary silicate mineral assemblage and the formation of a disseminated, fine-grained hematitic phase after the primary Fe oxides. Modally, there is a pronounced decrease in feldspar abundance toward the interior, commensurate with increases in the abundances of secondary feric minerals. As shown in Figure 2, the intrusion is divided into an interior zone of miarolitic albitite and an exterior zone of albitized monzonite. Relicts of a primary phenocryst assemblage that included andesine, hornblende, biotite, magnetite-ilmenite, and quartz are preserved in the exterior zone and allow for a detailed reconstruction of the original magmatic system. The boundary between the zones is taken as the last appearance of hornblende phenocrysts reckoned inward from the margins.

The alteration also involved metasomatic redistribution of K, Na, and Si as indicated by the sequence albite-anorthoclase/albite-orthoclase observed from core to margins in groundmass feldspars and, similarly, by the sequence albite-albite/oligoclase among the phenocryst feldspars. Loss of Ca from feldspars is balanced locally



Fig. 1. Location of Cuchillo Mountain.

Table 1. Modal analyses of the miarolitic fraction of the Cuchillo Mountain albite porphyry

	Exterior Zone*		Interior Zone*	
	1	2	3	4
	$\bar{x}(s)**$		$\bar{x}(s)**$	
Feldspar	4.60(3.24)	60.0	1.49(1.03)	20.4
Quartz(1)***	2.03(0.81)	26.5	1.96(0.78)	26.8
Quartz(2)***	0.04(0.04)	0.5	0.36(0.49)	4.9
Epidote	0.80(0.48)	10.4	2.49(1.91)	34.0
Chlorite	0.10(0.16)	1.3	0.36(0.36)	4.9
Calcite	0.10(0.19)	1.3	0.66(0.94)	9.0
Total	7.67	100.0	7.32	100.0

* Columns 1 and 3: means and standard deviations of modal abundances in volume percent; columns 2 and 4: mean values normalized to 100 %.

** Weighted means and standard deviations of seven analyses each from the exterior and interior zones. Total points per analysis ranged from 572 to 1451.

*** Quartz(1) refers to quartz in association with feldspars as illustrated in Types B-F miarolitic segregations of Figure 3. Quartz(2) refers to all other occurrences of quartz within the miarolitic segregations.

by modal increases in epidote; loss of Fe and Mg from primary mafic minerals is balanced locally by epidote-chlorite-hematite replacements.

PETROGRAPHY OF THE MIAROLES

Modal analyses

Modally, no difference in the total abundance of miarolitic segregations (7%), groundmass (48%), and phenocrysts (45%) is evident between the exterior and interior zones exclusive of chilled margins. However, the relative abundances of the component minerals of the miarole fraction vary significantly. Table 1 compares modal analyses of the miarolitic assemblage from the exterior and interior zones, expressed as absolute abundances and normalized equivalents. The trends shown are readily identified qualitatively and in general reflect a balance between a decrease in feldspar and an increase in hydrous feric minerals and carbonate toward the interior.

Textural relations

Figure 3 illustrates the principal types of miarolitic segregations, labeled A-F in order of first appearance inward from the intrusive margins. None of these features is observed in chilled margins; thus, they represent a post-placement assemblage. Each succeeding type incorporates

the textural elements of the preceding type, and as shown in Figure 4, as many as four types can coexist at the same location.

Type A segregations are simple polycrystalline quartz aggregates observed over a relatively limited range in near-margin rocks. The quartz extends with optical continuity into the interstices of the bounding groundmass-feldspar framework. Type B segregations are podlike aggregates of blocky feldspar grains disposed peripherally around quartz, which is characterized by linear inclusion trains. In some instances, skeletal blades of feldspar project into the quartz. Commonly, the quartz is a single grain in optical continuity with groundmass quartz beyond the margin of the pod. In all cases, the quartz is separated from the groundmass by the blocky feldspars. The transition from groundmass to pod is abrupt in terms of grain size and crystal

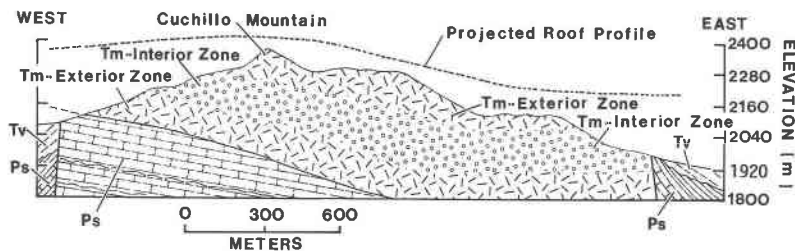


Fig. 2. Generalized section through the central portion of the albite porphyry intrusion. Tertiary volcanic rocks (Tv) are cogenetic with the albite porphyry (Tm); host rocks are Paleozoic sedimentary rocks (Ps). Roof profile is projected from outcrops out of the plane of the section.

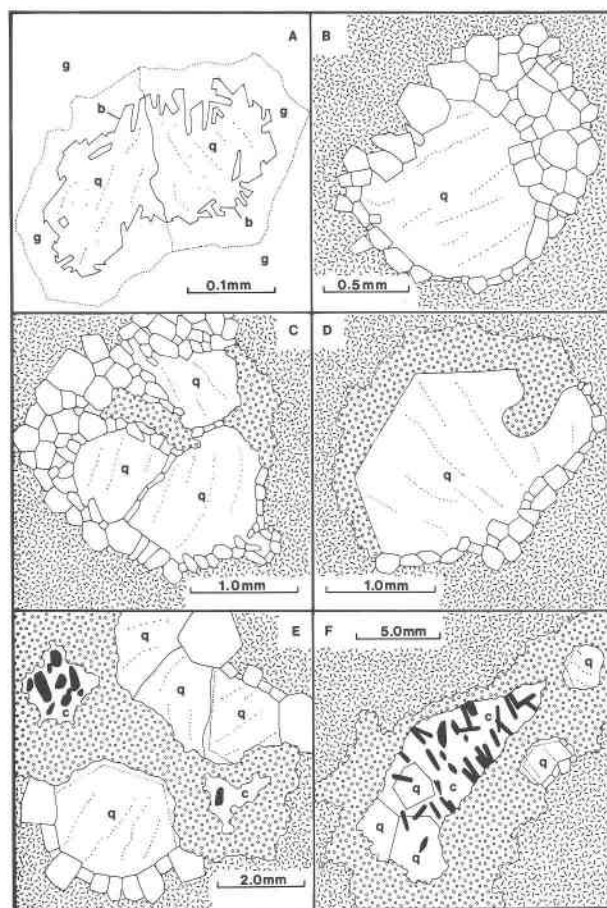


Fig. 3. Principal types (A–F; see text) of miarolitic segregations. Groundmass indicated by g or random dashes; quartz by q and inclusion trains; subhedral and euhedral epidote by black; domains of granular epidote \pm chlorite \pm calcite by circles; optically continuous fields of calcite by c; feldspar grains are unmarked. Dotted line in A indicates limits of optical continuity of quartz beyond the groundmass boundary (b), defined by fringing laths of feldspar.

habit. Type C segregations consist of several Type B units within irregular masses, wholly, or in part, enclosing domains of granular, subhedral epidote \pm chlorite, quartz, or interstitial calcite. This marks the first appearance of femic minerals within the miaroles, and it should be emphasized that these are primary crystals, not replacements of other femic grains. Type D segregations vary from simple podlike masses to irregular masses consisting of single or multiple quartz grains partially fringed by blocky feldspar grains and with euhedral faces against domains of granular epidote as in Type C. Type E segregations consist of multiple units of Type C and D and include fields of optically continuous calcite within granular epidote domains, hosting subhedral to euhedral epidote grains. Euhedral outlines within quartz grains are commonly marked by inclusions and epitaxially overgrown by another generation of quartz. Type F segregations are crystal-lined

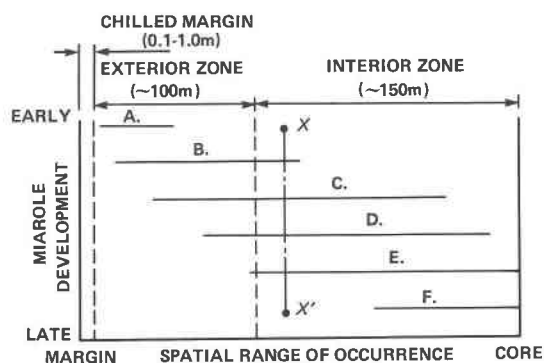


Fig. 4. Paragenetic model illustrating the spatial and temporal range of the miarole types identified in Figure 3.

cavities filled by optically continuous fields of calcite. The cavity margins are composed of granular subhedral epidote; the irregular outer fringe of this domain extends by replacement into the adjacent groundmass and phenocrysts. Type D units are found within the granular epidote wherein the feldspars are partially replaced. Crystals within the calcite-filled cavity are euhedral quartz and epidote; the earliest of these project into the cavity from "points of anchorage" on the inner margin of the granular epidote domain.

Figures 5 and 6 are detailed views from photomicrographs of a Type F interior-zone miarole. The euhedral epidote within the calcite-filled cavity exhibits two stages of crystallization exemplified by the relatively large crystals projecting inward from the cavity wall. The first stage is represented by turbid, irregular, and fractured grain interiors; the second stage is represented by clear epitaxial mantles forming the euhedral grain exteriors. Most fractures in the cores do not transect the overgrowths. The grain interiors are yellowish and slightly pleochroic in plane light with second-order interference colors under crossed nicols. The grain interiors are similar to the earlier epidote of the granular domain and to replacement epidote not associated with the miarolitic segregations. The mantles are colorless in plane light with first-order interference colors under crossed nicols. The mantles are similar to the population of internally homogeneous, doubly terminated euhedral crystals found in the center of the cavity.

Compositional relations

Determinations of SiO_2 , Al_2O_3 , Fe_2O_3 , CaO , and MnO in epidote, MnO in calcite and Na_2O , CaO and K_2O in feldspar were obtained using an ARL-EMX-SM electron microprobe operating at 15 kV and a sample current 0.03 μA . Standards employed were kaersutite (Si and Al), clinopyroxene (Ca, Fe, and Mn), albite (Na), bytownite (Ca), and orthoclase (K).

Analyses of cores and rims of crystals shown in Figures 5 and 6 are presented in Table 2. These data were reduced using the procedure of Bence and Albee (1968). They indicate that early epidote from the granular domain and

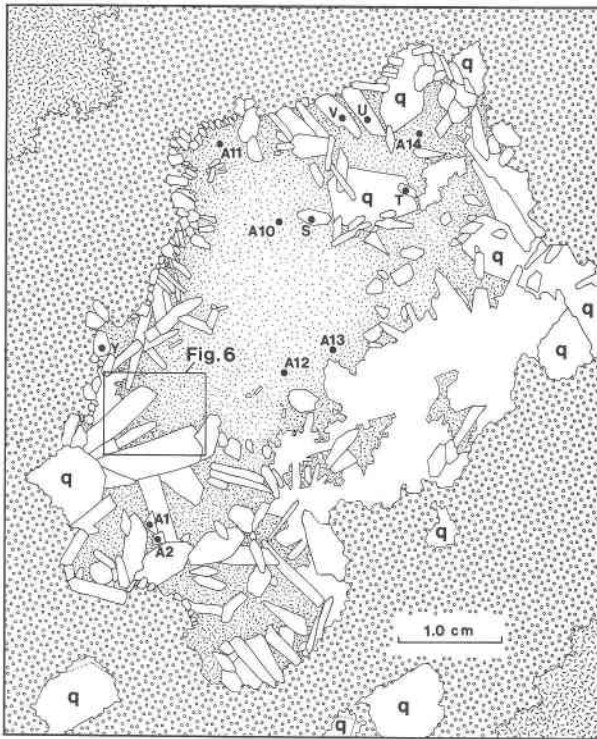


Fig. 5. Line drawing from photomicrographs of a Type F interior-zone miarole showing locations of electron-microprobe analyses presented in Table 2 and reported in text. Rectangle indicates area illustrated in Figure 6. Groundmass indicated by random dashes; granular epidote domain by circles; quartz by q; optically continuous calcite field by random dots; epidote euhedra and areas of undifferentiated euhedral grains are unmarked.

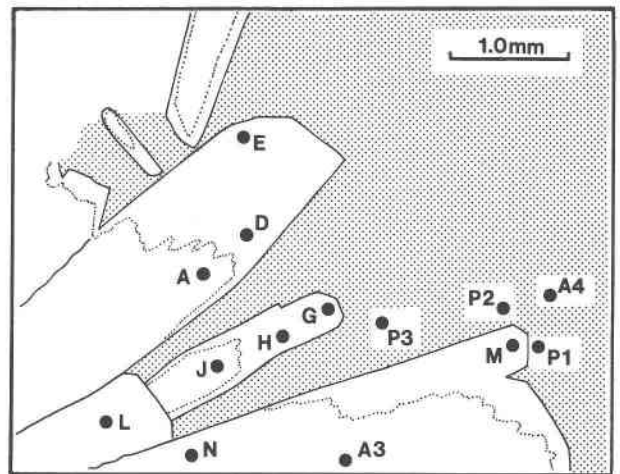
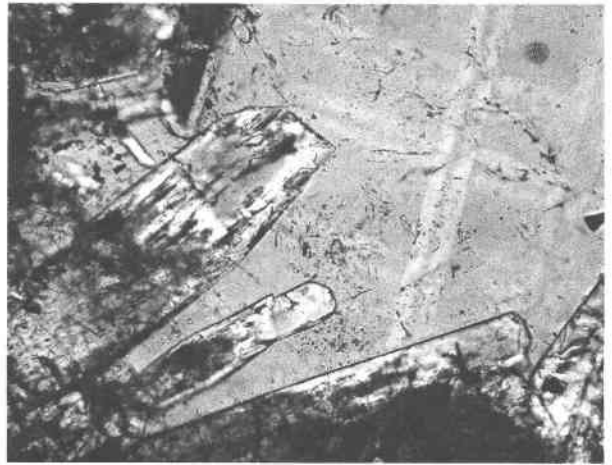


Fig. 6. Photomicrograph and line drawing of Figure 5 detail, showing location of electron-microprobe analyses (Table 2 and text). Contact between fractured cores and clear rims in epidote shown by dotted line; calcite by dots. Note calcite twinning in photo.

cores of overgrown crystals can be distinguished from more aluminous and manganiferous overgrowths and later, doubly terminated crystals. On average, differences are most apparent in MnO and Fe₂O₃, the overgrowths being higher in MnO (1.14 vs. 0.63 wt% and lower in Fe₂O₃ (12.16 vs. 13.25 wt%) than the cores. The more aluminous character of the overgrowths is shown by structural formulas indicating that the substitution of Fe for octahedrally coordinated Al is 23.6 mol% in rims and 26.1 mol% in cores. A similar trend is indicated by the results of partial microprobe analyses, XRD, and optical determinations of relatively early and late epidote from other Type E and F miaroles.

Wavelength scans of epidote grains in Figures 5 and 6 detected no elements in cores that were not also present in the rims. Scans were also made of euhedral quartz and the cavity-filling calcite. No impurities were detected in quartz, but both P and Mn were detected in calcite. Quantitative determinations of MnO in calcite were made at nine points shown in Figures 5 and 6. Comparison of the mean values of MnO (and their respective standard deviations, *s*) for early epidote (0.63 wt%, *s* = 0.15), late epidote (1.14 wt%, *s* = 0.51), and calcite (1.82 wt%, *s* =

0.24) reveals a trend of increasing MnO content within progressively later miarole products.

Bulk compositions of the phenocryst, groundmass, and miarole feldspar fractions of the albite porphyry were estimated from approximately 600 electron microprobe analyses of CaO, Na₂O, and K₂O recalculated in terms of the feldspar end members. Data corrections, other than for background and machine drift, were ignored since standards and unknowns were highly similar in composition. The results, plotted in Figure 7, are internally consistent and reflect the superposition of metasomatic changes on a primary fractionation trend, as later discussed. The miarole feldspars are K-rich (Or₇₀Ab₁₈An₃), optically homogeneous, and have a lower refractive index than the albitic feldspars of coexisting groundmass (exterior zone: Or₁₈Ab₇₅An₇; interior zone Or₁₈Ab₈₀An₂).

Table 2. Electron-microprobe analyses of oxides, in weight percent, and structural formulas of euhedral epidote from the Type F miarole illustrated in Figures 5 and 6

Rims*	D	E	G	H	M	S	T	U	V	$\bar{x}(s)$
SiO ₂	37.76	36.70	38.36	37.27	37.35	36.38	36.35	37.41	36.78	37.15(0.66)
Al ₂ O ₃	27.38	24.91	24.39	23.97	24.70	25.36	24.76	25.14	26.45	25.23(1.06)
Fe ₂ O ₃ **	8.28	12.66	11.37	11.62	12.77	13.36	13.80	13.38	12.20	12.16(1.66)
CaO	21.44	20.40	21.21	20.81	21.72	20.76	20.74	21.80	22.77	21.29(0.73)
MnO	1.03	1.85	0.43	0.94	0.68	1.68	1.68	0.71	1.30	1.14(0.51)
Total	95.89	96.52	95.76	94.61	97.22	97.54	97.33	98.44	99.50	96.97(1.48)
Number of cations on the basis of 12.5 oxygens										
Si	3.00	2.96	3.08	3.04	2.98	2.91	2.92	2.95	2.88	2.97
Al	0.00	0.04	0.00	0.00	0.02	0.09	0.08	0.05	0.12	0.03
	[3.00]	[3.00]	[3.08]	[3.04]	[3.00]	[3.00]	[3.00]	[3.00]	[3.00]	[3.00]
Al	2.58	2.34	2.32	2.32	2.31	2.31	2.27	2.30	2.33	2.36
Fe	0.50	0.77	0.69	0.72	0.77	0.81	0.84	0.80	0.72	0.73
	[3.08]	[3.11]	[3.01]	[3.04]	[3.08]	[3.12]	[3.11]	[3.10]	[3.05]	[3.09]
Ca	1.83	1.76	1.82	1.82	1.86	1.78	1.78	1.84	1.91	1.82
Mn	0.07	0.13	0.03	0.07	0.05	0.11	0.11	0.05	0.09	0.08
	[1.90]	[1.89]	[1.85]	[1.89]	[1.91]	[1.89]	[1.89]	[1.89]	[2.00]	[1.90]
Cores										
	A	J	L	N	Y	A1	A2	A3		$\bar{x}(s)$
SiO ₂	37.04	36.94	36.57	36.17	37.05	34.91	36.76	35.56		36.38(0.78)
Al ₂ O ₃	23.44	24.27	23.45	23.18	24.21	26.96	27.29	25.37		24.77(1.61)
Fe ₂ O ₃ **	12.67	12.62	14.34	13.90	15.79	11.88	11.98	12.84		13.25(1.33)
CaO	20.78	20.97	21.68	21.50	22.22	21.71	22.66	21.70		21.65(0.61)
MnO	0.78	0.66	0.49	0.59	0.42	0.89	0.65	0.55		0.63(0.15)
Total	94.71	95.46	96.53	95.34	99.69	96.35	99.34	96.02		96.68(1.85)
Number of cations on the basis of 12.5 oxygens										
Si	3.02	3.00	2.96	2.96	2.91	2.82	2.87	2.88		2.93
Al	0.00	0.00	0.04	0.04	0.09	0.18	0.13	0.12		0.07
	[3.02]	[3.00]	[3.00]	[3.00]	[3.00]	[3.00]	[3.00]	[3.00]		[3.00]
Al	2.27	2.33	2.21	2.21	2.17	2.39	2.39	2.31		2.29
Fe	0.78	0.77	0.88	0.86	0.94	0.72	0.70	0.79		0.81
	[3.05]	[3.10]	[3.09]	[3.07]	[3.11]	[3.11]	[3.09]	[3.10]		[3.10]
Ca	1.82	1.82	1.88	1.89	1.87	1.88	1.90	1.88		1.87
Mn	0.05	0.05	0.03	0.04	0.03	0.06	0.04	0.04		0.04
	[1.87]	[1.87]	[1.91]	[1.93]	[1.90]	[1.94]	[1.94]	[1.92]		[1.91]

*Includes internally homogeneous crystals in center of miarole.
 **Total Fe calculated as Fe³⁺.

DISCUSSION

All, or part, of the textural sequence illustrated in Figure 3 can be observed in any of three modes: (1) The sequence is evident in the distribution of miarole types from margin to core, hence from early to late in the consolidation history of the intrusion (Fig. 4). (2) The sequence is present among miarolitic segregations coexisting at a single locality, as represented on Figure 4 by the line $x-x'$. (3) The sequence is contained within individual complex miaroles of Types E and F. Thus, the quartz-feldspar aggregates in the near-margin rocks are clearly related to the femic aggregates of the core, representing respectively the initial and latest products of crystallization under vapor-saturated conditions. The textural sequence reflects the reciprocal, time-dependent relation between the relative abundances of melt and vapor, which (as is evident in Table 1) is expressed as a modal balance between quartz and feldspar of the exterior zone and hydrous femic minerals

and calcite of the interior zone. As subsequently discussed, it also reflects the extent to which the vapor and the saturated melt were mutually segregated at a given location, as a function of the cooling rate.

That the miaroles formed late in the consolidation history of the albite porphyry is indicated by the confinement of the miarolitic aggregates to available space within the postemplacement groundmass (representing nearly 50 vol% of the intrusion), from replacement of groundmass and phenocrysts by aggregates of miarolitic epidote and by the compositional trends of the feldspar fractions. This suggests that vapor saturation occurred late during post-emplacement crystallization. Because the emplacement depth was shallow (<2000 m, as indicated by reconstruction of the geologic section), the confining pressure was low; hence, it can be inferred that the water content of the system was relatively low (a confining pressure of 600 bars, or less, corresponds to a water content of 2.5 wt%,

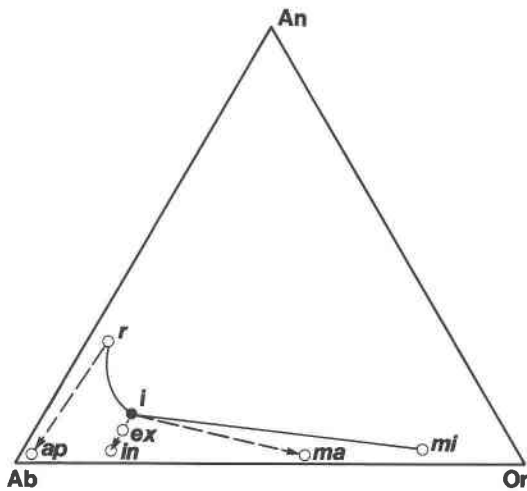


Fig. 7. Paragenetic model of feldspar crystallization and metasomatism. Relic phenocrysts (*r*); albitized phenocrysts (*ap*); hypothetical initial groundmass (*i*); exterior-zone groundmass (*ex*); interior-zone groundmass (*in*); near-margin groundmass (*ma*); miarole fraction (*mi*).

or less; Burnham and Jahns, 1962; Hamilton et al. 1964). This accords with Jahns and Burnham (1969, p. 855) who, in their model of the derivation of pegmatitic magma, viewed miaroles and related features as indicative of the transition from crystallization in a vapor-absent melt to crystallization in a vapor-saturated melt. Early saturation, at a given confining pressure, implies an increased potential for the large domain separation of hydrous melt and vapor; conversely, late saturation implies that such separation will be physically restricted and that the products of crystallization therefrom will be small and widely dispersed. In addition, late vapor saturation would tend to yield a pervasively distributed vapor phase within the nearly solidified magma, a condition that would promote reactions between the vapor and the primary mineral assemblage while at the same time allowing the development of miarolitic segregations.

At low confining pressures and low H_2O contents (conditions inferred for the albite porphyry), the temperature interval between vapor saturation of the melt and the solidus is small, as illustrated in the $T-X_{H_2O}$ phase-assemblage diagrams of Whitney (1975) and Naney and Swanson (1980). Hence, the length of time the system resides in the crystal + melt + vapor realm is important in determining the extent of separation of the vapor from crystals and melt. Since the rate of consolidation would have decreased toward the interior of the mass, according to the cooling model and attendant assumptions of Whitney (1975), segregation of the vapor phase should have been proportionately more complete in the interior zone compared to the exterior zone. The differential cooling rate between the interior and exterior parts of the intrusion is the primary control on the distribution of simple and complex miaroles within the albite porphyry.

The growth rate of crystals and the degree of perfection

of crystal faces within domains of vapor should have been high relative to crystals in the melt as a result of an increased ability of constituents to diffuse to crystal-vapor interfaces. Textures indicative of vapor-phase crystallization are found in the interior parts of Type E and F miaroles. These include euhedral epidote and quartz that project into spaces subsequently filled by calcite. Clear epidote overgrowths that mantle fractured and turbid cores in the euhedral grains of epidote within some miaroles represent a second stage of vapor-phase crystallization that followed crystallization and fracturing of the cores. This is evident from the fractures, nearly all of which do not transect the mantles. The epidote of the crystal cores is compositionally similar to epidote in the surrounding granular aggregates, but it is different in its MnO content and Fe-Al ratio from epidote of the overgrowths. These textural and compositional relationships are analogous to those observed in tourmalines from some pegmatite pockets (Foord, 1977) and have been explained as the result of thermal shock caused by pressure reduction during the rapid escape of vapor from the system (Jahns, 1982; Jahns, pers. comm.). Incomplete escape of vapor allows crystallization to resume under changed physical and chemical conditions. If such a mechanism were applicable to the albite porphyry intrusion, it would imply essentially closed-system behavior of the vapor phase. Local vapor-pressure reduction in the interior zone of the albite porphyry at the magmatic stage could be brought about by coeval faulting or fracturing in the already-consolidated parts of the body.

Gross trends in the composition of the vapor phase can be inferred qualitatively from the coexisting minerals of the miaroles. Initially, the anhydrous composition of the vapor phase would be described in terms of the system Ab-Or-Q, reflecting a melt composition near the granite minimum. At a later stage, the vapor phase coexisted with epidote, requiring Ca and Fe for which there is no other source than the decomposition of relatively An-rich feldspars and, to a lesser extent, primary mafic minerals. Figure 7 presents a model of feldspar decomposition. The open circles are measured compositions of the various feldspar fractions of the albite porphyry; the solid dot is an inferred composition representing the original groundmass. The solid line links the primary compositions, the dashed lines with arrows indicate the directions of subsequent metasomatism.

The primary paragenetic sequence of the albite porphyry (plagioclase + melt—plagioclase + alkali feldspar + melt—plagioclase + alkali feldspar + quartz + melt—plagioclase + alkali feldspar + quartz + melt + vapor) is in qualitative agreement with that of synthetic quartz monzonite for water contents less than 4.0 wt% at 2-kbar pressure (Whitney, 1975, p. 347). The primary feldspars ranged in composition from early-stage andesine, represented by point *r* measured from relict phenocrysts in the exterior zone, to intermediate-stage groundmass anorthoclase represented by point *i* (Fig. 7). The line *r-i* represents a primary fractionation trend. Late-stage crystalli-

zation is represented by the tie line between points *i* and *mi*, the latter point representing the K-rich feldspars of the miarolitic segregations. The original melt can be characterized as a relatively An-rich siliceous liquid yielding two feldspars. Primary crystallization trends can, therefore, be explained in terms of the system Ab-Or-An-Q (Carmichael, 1963) in which a fractionating melt first yields feldspars progressively enriched in K, then upon reaching the ternary feldspar minimum, yields a second, coprecipitating, series of feldspars progressively enriched in Na. The point *ap* represents the bulk composition of the albitized phenocrysts of the interior zone. The line *r-ap* indicates that the main effect of feldspar decomposition is the loss of An component. The measured points *ex* and *in* lie along a line parallel to *r-ap*, suggesting that the groundmass fraction behaved similarly. The assumption that the composition of the original groundmass lay near *ex* is justified by the preservation of primary relicts in the exterior zone. Point *i* was chosen such that it was distinct from *ex* for illustrative purposes. The point *ma* represents the measured groundmass composition in near-margin rocks derived from the loss of An and the gain of Or relative to *i*. The primary composition of the earliest groundmass feldspars, as represented in the chilled- and near-margin rocks, should either be similar to *i* or lie toward the Or side of *mi*.

Latest crystallization within the Type F miaroles does not reflect vapor-phase compositions characterized by K or Na, but rather by Ca, Fe, Mn, and CO₂, an elemental assemblage that is consistent with the femic replacement assemblage of the interior zone and with a highly evolved vapor phase. The carbonate fillings of the interior-zone miaroles apparently represent late-stage enrichment of the vapor in CO₂ as H₂O was being removed by OH-bearing phases. A genetic relationship between these miarole fillings is indicated by the enrichment of Mn in late-forming epidote and last-forming calcite.

The earliest miarolitic segregations predate the femic replacements of the interior zone; yet, the euhedral epidotes of the Type F miaroles record at least two stages of vapor-phase crystal growth later than the surrounding domains of granular epidote, which are primary at the cavity wall and secondary where they merge with surrounding groundmass and phenocrysts. This suggests that the development of the albite porphyry was to a significant extent a late magmatic effect.

ACKNOWLEDGMENTS

This paper was an outgrowth of a dissertation, completed at Stanford University and guided by the late Richard H. Jahns. I am grateful to Dick for his teaching, humor, and friendship. The manuscript benefited from discussions with D. G. Horton, J. D. O'Brient, and P. E. Long, and from editing and review by R. C. Ewing and J. A. Whitney. The original work was supported by the B. R. Morris Fellowship in Earth Sciences, the New Mexico Bureau of Mines and Mineral Resources, and grants-in-aid from the School of Earth Sciences, the Shell Fund, and the Department of Applied Earth Sciences.

REFERENCES

- Bence, A.E., and Albee, A.L. (1968) Empirical correction factors for the electron microanalysis of silicates and oxides. *Journal of Geology*, 76, 382-403.
- Burnham, C.W., and Jahns, R.H. (1962) A method for determining the solubility of water in silicate melts. *American Journal of Science*, 260, 721-745.
- Carmichael, I.S.E. (1963) The crystallization of feldspar in volcanic acid liquids. *Geological Society of London Quarterly Journal*, 119, 95-131.
- Foord, E.E. (1977) Famous mineral localities: The Himalaya dike system, Mesa Grande district, San Diego County, California. *Mineralogical Record*, 8, 461-474.
- Hamilton, D.L., Burnham, C.W., and Osborn, E.F. (1964) The solubility of water and effects of oxygen fugacity and water content on crystallization in mafic magmas. *Journal of Petrology*, 5, 1, 21-39.
- Jahns, R.H. (1982) Internal evolution of pegmatite bodies. In Petr Černý, Ed. *Granitic pegmatites in science and industry*, 293-327. *Mineralogical Society of Canada Short Course Handbook* 8.
- Jahns, R.H., and Burnham, C.W. (1969) Experimental studies of pegmatite genesis: I. A model for the derivation and crystallization of granitic pegmatites. *Economic Geology*, 64, 843-864.
- Jahns, R.H., McMillan, D.K., O'Brient, J.D., and Fisher, D.L. (1978) Geologic section in the Sierra Cuchillo and flanking areas, Sierra and Socorro Counties, New Mexico. *New Mexico Geological Society Special Publication* 7, 131-138.
- McMillan, D.K., and Jahns, R.H. (1978) Metasomatism in the Cuchillo Mountain laccolith, Sierra County, New Mexico. *Geological Society of America Abstracts with Programs*, 11, 280.
- Naney, M.T., and Swanson, S.E. (1980) The effects of Fe and Mg on crystallization in the granite system. *American Mineralogist*, 65, 639-653.
- Whitney, J.A. (1975) Vapor generation in a quartz monzonite magma; a synthetic model with application to porphyry copper deposits. *Economic Geology*, 70, 346-358.

MANUSCRIPT RECEIVED APRIL 11, 1985

MANUSCRIPT ACCEPTED NOVEMBER 15, 1985